Chalcogenide nanoparticles and organic photosensitizers for synergetic antimicrobial photodynamic therapy

Carlos Garin[a,b], Teresa Alejo[a,b;*], Vanesa Perez-Laguna[c,d], Martin Prieto[a,b], Gracia Mendoza[e,f], Manuel Arruebo[a,b,f], Victor Sebastian[a,b,f,*], Antonio Rezusta[c,d]

[a]Instituto de Nanociencia y Materiales de Aragón (INMA), CSIC-Universidad de Zaragoza, Zaragoza 50009, Spain
[b]Department of Chemical Engineering, University of Zaragoza, Campus Río Ebro-Edificio I+D, C/ Poeta Mariano Esquillor S/N, 50018 Zaragoza, Spain
[c]Department of Microbiology, Hospital Universitario Miguel Servet, 50009 Zaragoza, Spain
[d]Department of Microbiology, Preventive Medicine and Public Health, University of Zaragoza, 50009 Zaragoza, Spain
[e]Aragon Health Research Institute (IIS Aragón), 50009 Zaragoza, Spain.
[f]Networking Research Center on Bioengineering, Biomaterials and Nanomedicine, CIBER-BBN, 28029 Madrid, Spain

* Corresponding authors: Teresa Alejo: teresaal@unizar.es and Victor Sebastian: victorse@unizar.es

KEYWORDS: photodynamic therapy, organic photosensitizers, copper sulfide nanoparticles, antimicrobial effect, near-infrared light.

ABSTRACT

Synergistic antimicrobial effects were observed for copper sulfide (CuS) nanoparticles together with indocyanine green (ICG) in the elimination of wild type pathogenic bacteria (*Staphylococcus aureus* ATCC 29213 and *Pseudomonas aeruginosa* ATCC 27853) and

also opportunistic fungal infective yeast (*Candida albicans* ATCC 10231). Furthermore, large antibacterial effects were observed for clinical isolates of Methicillin-resistant *S. aureus* (MRSA) PFGE strain-type USA300. This efficient antimicrobial action was attributed to the combined extra- and intracellular generation of reactive oxygen species upon light irradiation. Instead of the use of visible-light for the activation of common photosensitizers, both ICG and CuS nanoparticles can be activated in the near infrared (NIR)-region of the electromagnetic spectrum and therefore, superior tissue penetration would be expected in a potential elimination of pathogenic microorganisms not only on the skin but also in the soft tissue. In the different bacteria studied a 3-log reduction in the bacterial counts was achieved after only 6 min of NIR irradiation and treatment with ICG or CuS alone at concentrations of 40 and 160 μg/mL, respectively. A maximum bactericidal effect against *S. aureus* and USA300 strains was obtained for the combination of both photosensitizers at the same concentration. Regarding *P. aeruginosa,* a 4-log reduction in the CFU was observed for the combination of CuS and ICG at various concentrations. In *Candida albicans* the combination of both ICG and CuS and light irradiation showed an antimicrobial dose-dependent effect with the reduction of at least 3-log in the cell counts for the combination of ICG+CuS at reduced concentrations. The observed antimicrobial effect was solely attributed to a photodynamic effect and any photothermal effect was avoided to discard any potential thermal injury in a potential clinical application. The generation of reactive oxygen species upon near infrared-light irradiation for those photosensitizers used was measured either alone or in combination. The cytocompatibility of the proposed materials at the doses used in photodynamic therapy was also demonstrated in human dermal fibroblasts and keratinocytes by cell culturing and flow cytometry studies.

1 Introduction

Photodynamic therapy (PDT) is a minimally invasive therapeutic approach in which photochemical processes are induced by the combination of light, tissue oxygen and organic photosensitizers (*i.e.*, porphyrins, chlorophylls and dyes). Those processes induce the local cytotoxic generation of Type I (radicals and reactive oxygen species, ROS) and Type II (singlet oxygen) oxidation photoreactions in the irradiated area. The photosensitized oxidation generates those non-specific short-lived reactive species and, simultaneously, a battery of antioxidant cellular enzymes (i.e., catalase, superoxide dismutase, glutathione reductase, etc.) against Type I radicals try to counteract this oxidative stress. When the amount of oxidative species is high enough, peroxidation of cellular constituents such as proteins, lipids and nucleic acids takes place with the consequent cellular lysis.[1]

The Food and Drug Administration (FDA) has approved the use of PDT to treat or relieve the symptoms of esophageal cancer and non-small cell lung cancer and also to reduce the severity of skin symptoms of cutaneous T-cell lymphoma that has not responded to other therapies by using extracorporeal photopheresis.[2] Some skin and eye conditions such as actinic keratoses and macular degeneration, respectively, are also currently treated by means of PDT. Off-label applications of PDT include aesthetic indications, skin rejuvenation, psoriasis, arthritis, restenosis, Barrett's esophagus, antimicrobial treatments, to mention a few.[3]

Different photosensitizers have been used in the management of pathogenic microorganisms. The interaction of photosensitizers with Gram-positive or Gram-negative bacteria can be maximized by controlling the polycationic nature of the photosensitizer used, its ability to form H-bonds, and its hydrophilic/hydrophobic balance.[4] Photosensitizers can interact with bacteria using lipid-mediated pathways when

hydrophobic in nature, and by diffusion through porins when using hydrophilic ones. Anionic photosensitizers are internalized within bacterial cells by means of electrostatic interactions and protein transporters whereas cationic ones depend on electrostatic interactions and self-promoted uptake pathways.[5] Cationic photosensitizers are able to destabilize the lipopolysaccharides (LPS) constituting the outer membrane of Gram-negative bacteria by displacing the Mg^{2+} and Ca^{2+} groups which act as bridges between LPS molecules.[4] They are also able to destabilize the cell wall (peptidoglycan) structure in Gram-positive bacteria and to interact with the components of fungi cell wall (glucosamine polymer chitin, lipoproteins and glucan) producing lipid peroxidation, photodegradation of cell-membrane forming bonds, and inactivating cell-wall proteins.[6] The great advantage of antimicrobial PDT is not only its broad spectrum of application but also that the probability to develop resistance is minimized because multiple antimicrobial mechanisms of action take place simultaneously and therefore, multiple cellular mutations or over-expression of efflux pumps to counterbalance its action would be unlikely. Also, the photosensitizer does not need to be internalized in the targeted microorganism, but just located in its close proximity to exert inactivation without intracellular uptake and, therefore, its ability to drive resistance would also be minimized. Different attempts have been carried out *in vitro* to analyze the potential induction of bacterial resistance to different photosensitizers but they have shown no development of resistance, although those studies were conducted on planktonic bacteria and further research should focus on studying the effect on bacterial biofilms.[7] Finally, a spatiotemporal control of the therapy is applied in a restricted area on demand only when illuminating, reducing potential unwanted side effects in healthy tissues.

Several organic photosensitizers have been combined with antibiotics,[8-10] inorganic salts,[11] Fenton reagents,[12] metal ions,[13] etc. to promote a synergetic antimicrobial action.

Several others have been conjugated to antibodies,[14, 15] bacteriophages[16] or antimicrobial peptides[17, 18] in order to achieve a targeted delivery of the photosensitizer towards the pathogenic microorganism. Several innovative supramolecular photosensitizers, synthesized using host-guest chemistry, can exert their antimicrobial action on demand only when illuminated while being innocuous in the dark.[13] In addition to all those advanced systems, in clinical dentistry is nowadays approved the treatment of periodonto-pathogenic bacteria by PDT as an adjunct to periodontal therapy[19] and several antimicrobial photosensitizers have recently entered into clinical trials.[20]

However, despite all those advances, organic photosensitizers show several limitations: i) photobleaching, ii) the need of close proximity between the targeted microorganism and the photosensitizer (*i.e.*, in the order of a few tenths of nanometers[21]), iii) low singlet oxygen quantum yield, and iv) reduced biocompatibility and/or water solubility. Photobleaching is a light-dependent mechanism produced when the generated ROS or singlet oxygen react with the ground-state sensitizer deteriorating its structure.[22] To overcome some of those previous limitations, specially photobleaching, nanoparticles have been used as an alternative to organic photosensitizers. In this regard, stand-alone metal nanoparticles (*e.g.*, gold, silver, etc.), upconversion nanoparticles (*i.e.*, rare-earth based lanthanide- or actinide-doped transition metals), carbon nanomaterials (fullerenes, carbon nanotubes and graphene) and large band-gap semiconductor nanoparticles (*e.g.*, zinc oxide, titanium oxide, copper oxide, quantum dots, etc.) have been studied in the photodynamic elimination of pathogenic microorganisms.[23, 24] Conjugates based on nanoparticles and organic photosensitizers have also been proposed as efficient photodynamic agents to take advantage of the benefits of both materials. In those conjugates, the inorganic host can be used to avoid aggregation and self-quenching of the organic photosensitizer,[25] to drive it towards a specific pathological region[26] to collect it

after use[27] or to improve its solubility.[28] In other applications the additive or synergetic effect of both materials is combined to enhance their therapeutic action. In this regard, Shrestha *et al.*[29] demonstrated in the treatment of periodontal disease that by combining chitosan nanoparticles and Rose-Bengal a simultaneous antimicrobial effect and an increased stabilization of the integrity of the dentin hard-tissue by photo-crosslinking were achievable. Li *et al.*[30] demonstrated that multidrug resistant (MDR) bacteria can be eliminated from murine Methicillin-resistant *S. aureus* (MRSA)-infected abscesses even in the deep tissue (1 cm) by the combinatorial use of upconversion nanoparticles loaded with the photosensitizer zinc phthalocyanine. We demonstrated that by combining near-infrared (NIR)-activated upconversion nanoparticles and protoporphyrin IX, visible light can be generated in the deep tissue triggering the photooxidation of the organic photosensitizer in an *ex vivo* human-skin-permeation model.[31] Antibacterial (against MRSA and MDR *Escherichia coli*) and antifungal (against *Candida albicans*) effects have also been demonstrated *in vivo* by combining upconversion nanoparticles with photosensitizers (*i.e.*, carboxyphthalocyanine zinc).[32] Nanoparticles are also combined with photosensitizers in theragnostic platforms where the nanoparticle can act as a photosensitizer carrier and also as contrast agent in different medical imaging technologies. For instance, Zhou *et al.*[33] described the application of silver-coated gold nanoparticles used as Surface Enhanced Raman Scattering (SERS)-active cores coated with silica as a host of a photosensitizer (2,3-naphthalocyanine dihydroxide), and surface functionalized with vancomycin for the *in vitro* imaging of the binding ability of the nanoconstructs, as an alternative approach to fluorescence-based bacterial labeling, and for the *in vivo* photodynamic treatment of vancomycin-resistant enterococci strains. Finally, nanoparticles can also be used for the combined photodynamic and photothermal treatment of pathogenic microorganisms. As an example, Yuan *et al.*[34] described the use

of mesoporous polydopamine nanoparticles, having photothermal ability, containing indocyanine green (ICG) and surface functionalized with the Arg-Gly-Asp (RGD) peptide to promote cytocompatibility in an *in vivo* antibacterial validation on biofilms colonizing titanium-based implants. Other advanced antimicrobial and antiviral materials are based on nanofibrous membranes loaded with photosensitizers.[35] When photodynamic materials are encapsulated within fibers, their antimicrobial properties can be enhanced due to the improved stability, compatibility with biological environments, and a prolonged photosensitizer life-time. A recent work demonstrated the efficient antimicrobial activity of electrospun fibers based on Eudragit L100 loaded with curcumin.[36] Contreras *et al.*[37] developed fibrous scaffolds using electrospinning from FDA-approved polymers, either poly(ε-caprolactone (PCL) or poly[lactide-co-glycolide] (PLGA), containing different photosensitizers for the elimination of *Escherichia coli* under visible light exposure.

Despite all those advances in the field, most of the approaches described above include non-biodegradable metal, upconversion or semiconductor nanoparticles. Herein, we have proposed the combined use of the FDA approved ICG with chalcogenide nanoparticles based on copper sulfide (CuS). Preclinical data showed that, compared to persistent metal nanospheres (*e.g.*, gold), CuS nanoparticles are rapidly cleared from the body following the hepatobiliary route.[38] CuS nanoparticles have a dual photothermal and photodynamic ability and biodegrade by forming soluble copper sulfates.[39] Their combined antibacterial and antifungal (against *C. albicans*, a dimorphic pathogenic fungus/yeast) action is here demonstrated using *Pseudomonas aeruginosa* as a model of Gram-negative bacteria and different strains of *Staphylococcus aureus* including clinical isolates of MRSA as models of Gram-positive bacteria. Compared to other ultraviolet (UV)- or visible (VIS)-activatable photosensitizers, NIR-light activatable biodegradable nanomaterials were

chosen in order to reach deeper penetration in tissues in a potential future clinical application.[40] The final goal of the study is to demonstrate a synergetic effect by combining the bactericidal effect produced by CuS alone attributed to lipid peroxidation reactions and its efficient ROS generation together with the combined NIR-triggered photodynamic effect for both CuS and ICG boosting ROS production.

2 Experimental

2.1 Strains and chemicals. *Staphylococcus aureus* ATCC 29213 and *Pseudomonas aeruginosa* ATCC 27853 were obtained from Ielab (Spain). Columbia blood agar was purchased from Oxoid. Methicillin-resistant *S. aureus* (MRSA) PFGE strain type USA300 (multilocus sequence type 8, clonal complex 8, staphylococcal cassette chromosome mec type IV, namely ST8-USA300) was kindly donated by Cristina Prat MD-PhD, Institut d'Investigació en Ciències de la Salut Germans Trias i Pujol (IGTP, Spain). Tryptone soy broth (TSB) was purchased from Laboratorios Conda-Pronadisa S.A. (Spain). *Candida albicans* ATCC 10231 was obtained from the American Type Culture Collection (ATCC; Rockville, MD). All bacterial strains and yeast were cultured at 37ºC.

All the chemicals used in the synthesis (polyvinylpyrrolidone K30 (Mw 40000 Da); copper(II) chloride dihydrate (ACS reagent ≥99.0%); sodium sulfide nonahydrate (ACS reagent ≥98%); hydrazine (35 wt. % in water); sodium hydroxide (ACS reagent ≥97%,); Dihydrorhodamine 123 (>95%); and indocyanine green (Cardiogreen powder, ICG) were purchased from Sigma-Aldrich. Singlet Oxygen Sensor Green (SOSG) was purchased from Thermo Fisher Scientific.

2.2 Materials synthesis and characterization. The synthesis of CuS nanoparticles was performed following the work of Ramadan *et al.*[41] but scaling up their production.[42] In an open flask, 1.2 g of PVP K30 was dissolved in 125 mL of distilled de-ionized (DDI) water

at 70ºC and 500 µL of a 0.5 M solution of $CuCl_2$ and 125 mL of NaOH solution with its pH adjusted to 9 were added. Next, 32 µL of hydrazine solution was added under stirring, leading to the formation of CuS seeds; finally, 1 mL of Na_2S (320 mg/mL) were added to the previous dispersion, and kept under heating at 70ºC for 2h. The resulting nanoparticles were washed three times by centrifugation (6000 rpm, 10 min) and re-dispersed in DDI water at the desired concentration.

The optoelectronic properties of CuS nanoparticles and ICG were evaluated by means of UV−VIS absorption in a UV−vis−NIR spectrophotometer (Jasco V670, Tokyo, Japan). The heating efficiency of nanoparticle-based water suspensions and ICG solutions in water were measured after irradiating them with an 808 nm wavelength laser diode (6×8 mm^2 spot size; Optilas model MDL-III-808-2W, Changchun New Industries Optoelectronics Technology Co., Ltd., Changchun, China) and a power controller (Model PD300-3W, Ophir Laser Measurement Group, Logan, UT, USA) with varied fluences. Temperature increase was monitored using a K-type thermocouple (RS Amidata, Madrid, Spain) immersed in the dispersion/solution away from the laser path. The zeta potential of CuS-based suspensions was measured in a Brookhaven 90Plus particle size analyzer (Brookhaven Instruments Corp., Holtsville, NY, USA) using the ZetaPALS software in 1 mM KCl aqueous solution at pH = 6.5 and 25 ± 0.1 ºC. Zeta potential was determined by studying their electrophoretic mobility and then applying the Smoluchowski equation. The hydrodynamic diameter of aqueous CuS nanoparticle dispersions was evaluated by dynamic light scattering (DLS) in the same equipment. The morphology of the nanoparticles was observed by transmission electron microscopy (TEM; FEI Tecnai T20, operating at 200 kV).

ROS generation was indirectly evaluated using the non-fluorescent dye dihydrorhodamine 123 (DHR123) that under the presence of ROS is oxidized to

fluorescent rhodamine (R123). R123 fluorescence emission under the presence of the ICG and/or CuS nanoparticles in the presence or absence of NIR light were measured at 530 nm in a fluorescence spectrometer (Perkin Elmer Luminescence Spectrometer Model LS-55, Massachusetts, USA) using an excitation wavelength of 485 nm based on our previous experience.[39] Neither CuS nanoparticles nor ICG yielded fluorescence at the wavelength of 530 nm under the assayed conditions. ICG solution (40 μg/mL), CuS nanoparticles suspension (40 μg/mL) and ICG+CuS (40+40 μg/mL) were prepared in 1 mL ethanol containing 1.65 μM DHR123. The solutions were irradiated at 1 W/cm^2 (at 808 nm) during 6 min to study the ROS generation upon irradiation. Control experiments were carried out in the absence of light but heating the solutions at the same heating rate observed during the irradiation experiments. Singlet oxygen ($^1O_2$) generation was assessed using the commercially available fluorescent sensor named Singlet Oxygen Sensor Green (SOSG) which is highly selective for singlet oxygen. SOSG is provided in vials containing 100 μg of product. The 100 μg of solid SOSG were dissolved in 33 μL of methanol to obtain a stock solution of about 5 mM according to the manufacturer instructions. 1 μL of an intermediate stock solution of 400 μM SOSG in methanol were added to the ICG (40 μg/mL) or CuS (40 μg/mL) water solutions to have 200 μL of solution with a SOSG concentration of 2 μM. The samples were then irradiated by NIR light (808 nm, 1 W/cm^2) during 6 minutes and the fluorescence change was recorded with an excitation wavelength of 488 nm and an emission wavelength of 530 nm using a microplate reader (Multimode Synergy HT Microplate Reader; Biotek, USA). Fluorescence was also measured in the same samples without irradiation as control.

Photobleaching was induced by irradiating ICG solutions (400 μg/mL) at 808 nm during 3 min using an irradiance of 1 W/cm^2. As control, the same experimental conditions were used on an aqueous suspension (400 μg/mL) of CuS nanoparticles.

2.3 In vitro photodynamic studies. Selected bacteria (*S. aureus* ATCC 29213, USA300-(MRSA) and *P. aeruginosa* ATCC 27853) were seeded on blood agar and cultured overnight. Stock inoculum suspensions were prepared in DDI water and adjusted to optical densities corresponding to 0.5 ± 0.03 McFarland scale which for these microorganisms corresponds approximately to 10^8 cell/mL.[43] For *C. albicans*, the same process was used to prepare the stock inoculum suspensions, but then they were adjusted to 5.0 ± 0.03 McFarland scale, which for yeasts corresponds approximately to 1~5 x 10^6 cell/mL.

Afterwards, 90 µL of the prepared inoculums were replenished with 10 µL of varied concentrations of the photosensitizers (ICG, CuS nanoparticles or both) in Eppendorf tubes. The photosensitizer concentrations tested were 5-40 µg/mL for ICG, 10-160 µg/mL for CuS nanoparticles and 10/10, 10/160, 40/10, 40/40, 40/160, 20/80 µg/mL for ICG+CuS. Irradiation was then carried out using a laser irradiance of 1 W/cm^2 during 3 or 6 minutes (*i.e.* 180 J/cm^2 or 360 J/cm^2 respectively). After irradiating serial dilutions of aliquots of the treated samples were prepared and plated. Colony-forming units (CFU) were counted after 24h. As control samples, first we exposed samples without photosensitizer to the same irradiances, to evaluate if the laser could produce any antimicrobial effect by itself and no cytotoxic effect was observed (results not shown). Heating evolution was also evaluated to discard any potential cytotoxic effect attributed to a temperature increase because laser irradiances and photosensitizer concentrations were selected to avoid any photothermal damage. In parallel to the irradiated samples, identical samples were kept in the dark to evaluate the potential cytotoxicity of the photosensitizers at the doses used. Samples and controls were cultured on blood agar and incubated overnight at 37ºC. The effectiveness of the photodynamic treatment was assessed by the microdilution method by plating and counting the number of CFU/100µl

using a Flash and Go automatic colony counter (IUL, S.A, Spain) and comparing the results with those retrieved for the untreated controls. All experiments were carried out at least 3 times. All data were analyzed with Graphpad 8.0.2 using the two-ways analysis of variance (ANOVA) to determine the statistical significance of the results.

Moreover, bacteria morphology was also evaluated before and after treatment with the most effective concentration of ICG and CuS nanoparticles obtained from the assays described above. After treatment with ICG and CuS nanoparticles, samples were irradiated for 6 min and prepared for scanning electron microscopy (SEM) observation as previously reported.[44] In brief, samples were washed in 0.1 M PBS, fixed in 2.5% glutaraldehyde (90 min), filtered (0.2 μm, pore size cutoff) and finally dehydrated in ethanol series (30-100%; twice for 15 min). SEM micrographs were acquired by using a SEM Inspect F50 (FEI Co., Holland) operating at an accelerating voltage of 10 kV after mounting the samples on aluminum stubs using carbon tape and sputtered with a thin layer of carbon to make them conductive.

2.4 Cell viability and flow cytometry studies. ICG and CuS nanoparticles were *in vitro* tested in cell cultures in order to elucidate their cytocompatibility regarding their potential use as photodynamic therapy in skin and soft tissue associated infections. Considering this potential application, the cell lines assayed were human dermal fibroblasts (Lonza, Belgium) and HaCaT human keratinocytes (kindly donated by Pilar Martín-Duque PhD). Both cell types were cultured in Dulbecco's modified Eagle's medium (DMEM) high glucose containing stable glutamine (Biowest) and supplemented with fetal bovine serum (FBS, 10% (v/v), Thermo Fisher Scientific, MA) and antibiotic-antimycotic (60 μg/mL penicillin, 100 μg/mL streptomycin, and 0.25 μg/mL amphotericin B, Biowest). Cells were grown under humidified atmosphere containing 5% CO_2 at 37°C.

In vitro cytotoxicity of ICG and CuS nanoparticles was analyzed by means of the Blue Cell Viability assay (Abnova, Taiwan). Human dermal fibroblasts and keratinocytes were seeded in 96-well plates (6000 cells/well) and incubated with ICG (20-160 µg/mL) and CuS nanoparticles (40-320 µg/mL) at two different time points: 6 min (time used in the bacterial assays) and 24 h. After incubation, the reagent was added to the cells (10% v/v) and incubated for 4 h (37 ºC, 5% CO_2). Finally, the fluorescence was recorded (535/590 nm ex/em) in a Synergy HT microplate reader (Biotek, US). Cell viability was then calculated by interpolation considering that control samples (untreated cells) exerted 100% viability. Each viability percentage was obtained from five independent experiments. Furthermore, the potential ICG and CuS nanoparticle interference with the methodology was tested and discarded.

Flow cytometry studies were developed in order to elucidate the effects of ICG and CuS nanoparticles on fibroblasts and keratinocytes. At the subcytotoxic concentrations found in the viability assay described above and after incubation for 24 h (37 ºC, 5% CO_2), cell samples were analyzed by flow cytometry regarding cell apoptosis and cycle. In brief, apoptosis was evaluated by cell staining with annexin V-FITC, propidium iodide and annexin V binding buffer, to be then further incubated in binding buffer for 15 min and analyzed in a FACSARIA BD equipment through the FACSDIVA BD software. Conversely, the distribution of cell cycle phases after treatment was studied after fixing cells in 70% ice-cold ethanol and DNA staining mediated by RNase A and propidium iodide. Then, cell samples were analyzed in a FACSARRAY BD equipment with the MODIFIT 3.0 Verity. In both flow cytometry studies, control samples were also analyzed to test cellular basal status and compare it with those obtained with the treated cells.

3 Results and discussion

Fig. 1a,b shows the morphology of the resulting CuS nanoparticles. These nanoparticles depict a hollow structure with a wall thickness of approximately 40 nm. The hollow structure is caused by a Kirkendall diffusion effect during the nanoparticle synthesis, where sulfur atoms diffuse into the Cu_2O template nanoparticles at the same time that copper atoms diffuse outwards.[39] The zeta potential obtained for CuS nanoparticles was -17.48 ± 0.83 mV (pH=6.5) and DLS analysis revealed hydrodynamic particle sizes centered at 200 ± 30 nm whereas the analysis from TEM images showed sizes around 185 ± 20 nm in agreement with the previous literature.[39, 41] The induced accelerated photobleaching of ICG in water after being irradiated for 3 min with an 808 nm laser at 1 W/cm^2 (Fig. 1c,d and insets) clearly showed the disappearance of its representative absorption peaks at 710 and 780 nm characteristic of dimers formation at concentrations above 0.1 μM.[45] The insets clearly show how the characteristic green color of ICG is rapidly lost after irradiation. Under the same irradiance and exposure time the absorption spectrum of CuS nanoparticle aqueous suspensions remained unchanged (Fig. 1e,f). Those semiconductor CuS nanoparticles showed a maximum absorption in the spectra at 1050 nm characteristic of their covellite structure.[39] We have previously shown that those nanoparticles remain unaltered after repeated cycles of irradiation maintaining their ability of absorbing incident NIR light.[39] Heating effects were also evaluated for ICG aqueous solutions (40 μg/mL) during 6 minutes of irradiation at 808 nm (1 W/cm^2) and for CuS aqueous suspensions (160 μg/mL) under the same conditions. ICG and CuS increased the solution temperature in ~12º and 4ºC, respectively (Fig. 1g,h). The heating curve of combined ICG+CuS 40+40 μg/mL during 6 minutes of irradiation at 808 nm (1 W/cm^2) exhibited a temperature increase equivalent to the one of the ICG solution alone at the same concentration (Fig. S1). In order to decouple the photodynamic from the

photothermal effect, control experiments on the cellular viability of the pathogenic microorganisms studied *(S. aureus*, *P. aeruginosa*, MRSA and *C. albicans*) were performed increasing the cultures temperature up to 15ºC without observing any reduction in the CFU counts ~~(results not shown)~~ indicating that any loss in cell viability would be attributed to a mere photodynamic effect. The results of the tests performed in order to evaluate if the pathogenic *S. aureus* could be eliminated in a flash thermal ablation, simulating the conditions reached during the photodynamic assay, are shown in Table S1. As it is observed, the colonies were incubated at 52 ºC during 5 and 20 min but no relevant cell death was observed. Other research groups have demonstrated that *S. aureus* has high thermal resistance as it takes more than 530 min to eliminate it at 54.4ºC.[46]

In a clinical setting a thermal effect would be disadvantageous due to the potential generation of necrotic tissue (*e.g.*, eschar) and a subsequent delayed cell proliferation, hindered migration, regeneration and remodeling of connective tissue to restore skin integrity and strength. For that reason, we focus exclusively on generating PTD effects.

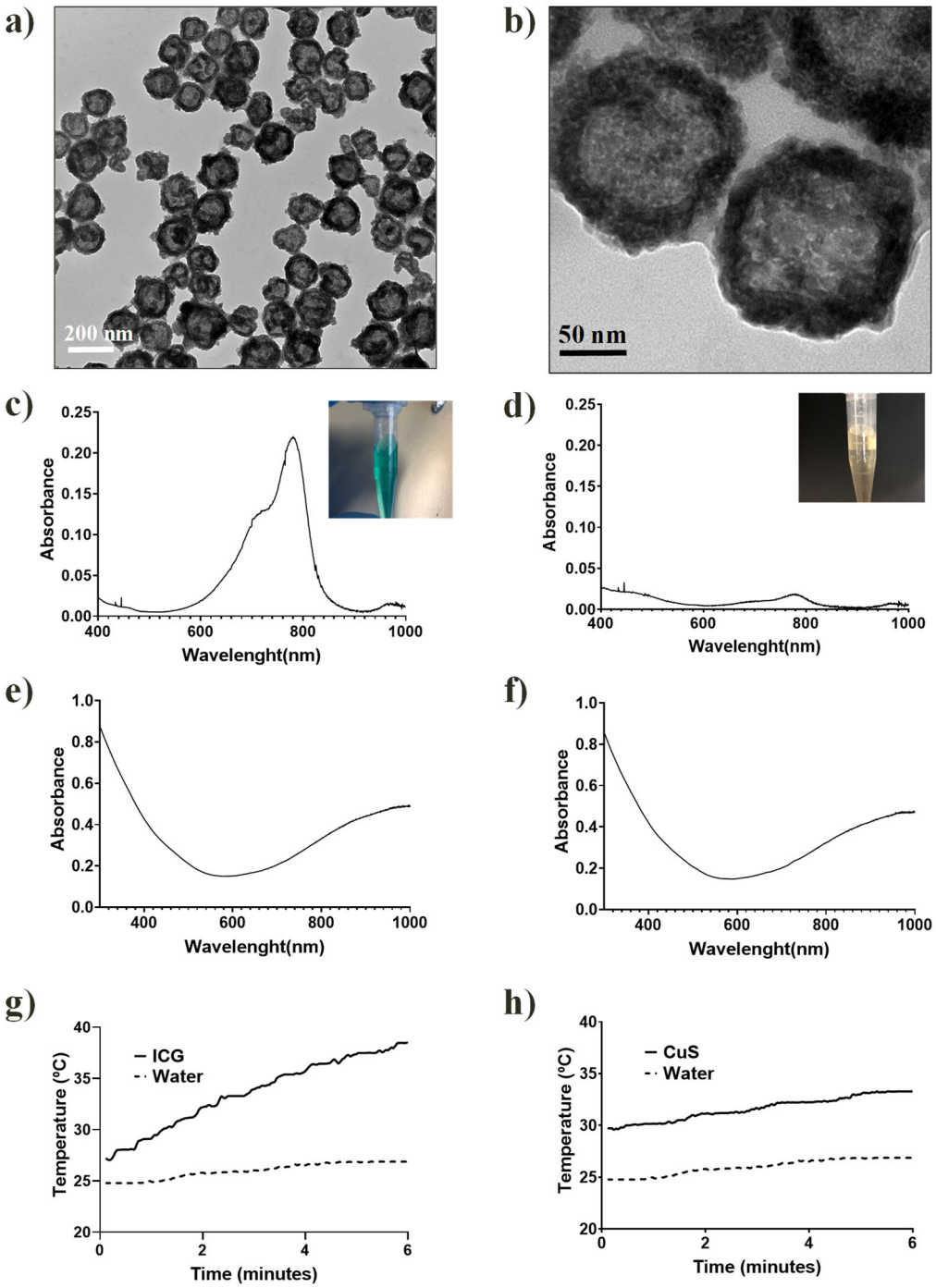

Fig. 1. (a) and (b) TEM images of CuS NPs. (c) Absorption spectrum of an ICG solution before being irradiated. (d) Absorption spectrum of the same ICG solution after being irradiated for 3 min with an 808 nm laser with an irradiance of 1 W/cm^2. (e) Absorption spectrum of a CuS NPs solution before being irradiated. (f) Absorption spectrum of the same CuS NPs solution after being irradiated for 3 min (808 nm, 1 W/cm^2). (g) Heating

curve of ICG 40 μg/mL and water control during 6 minutes (808 nm, 1 W/cm^2). (h) Heating curve of CuS 160 μg/mL and water control during 6 minutes of irradiation (808 nm, 1 W/cm^2).

CuS nanoparticles absorb NIR light due to the excitation of direct (band-to-band) transitions, indirect transitions, and plasmonic photoexcitation.[47] We have previously demonstrated that CuS nanoparticles are able to generate ROS after NIR-light illumination.[39] On the other hand, part of the energy absorbed by ICG after NIR irradiation is converted into 830 nm-fluorescent light (fluorescence quantum yield in albumin solution is reported around 4%), part is transferred to its triplet T1 state generating reactive oxygen species and part is internally converted into heat (around 85% of the absorbed light).[48] Therefore, the combination of both CuS nanoparticles and ICG could boost ROS generation and its consequent oxidative stress and microbial damage.

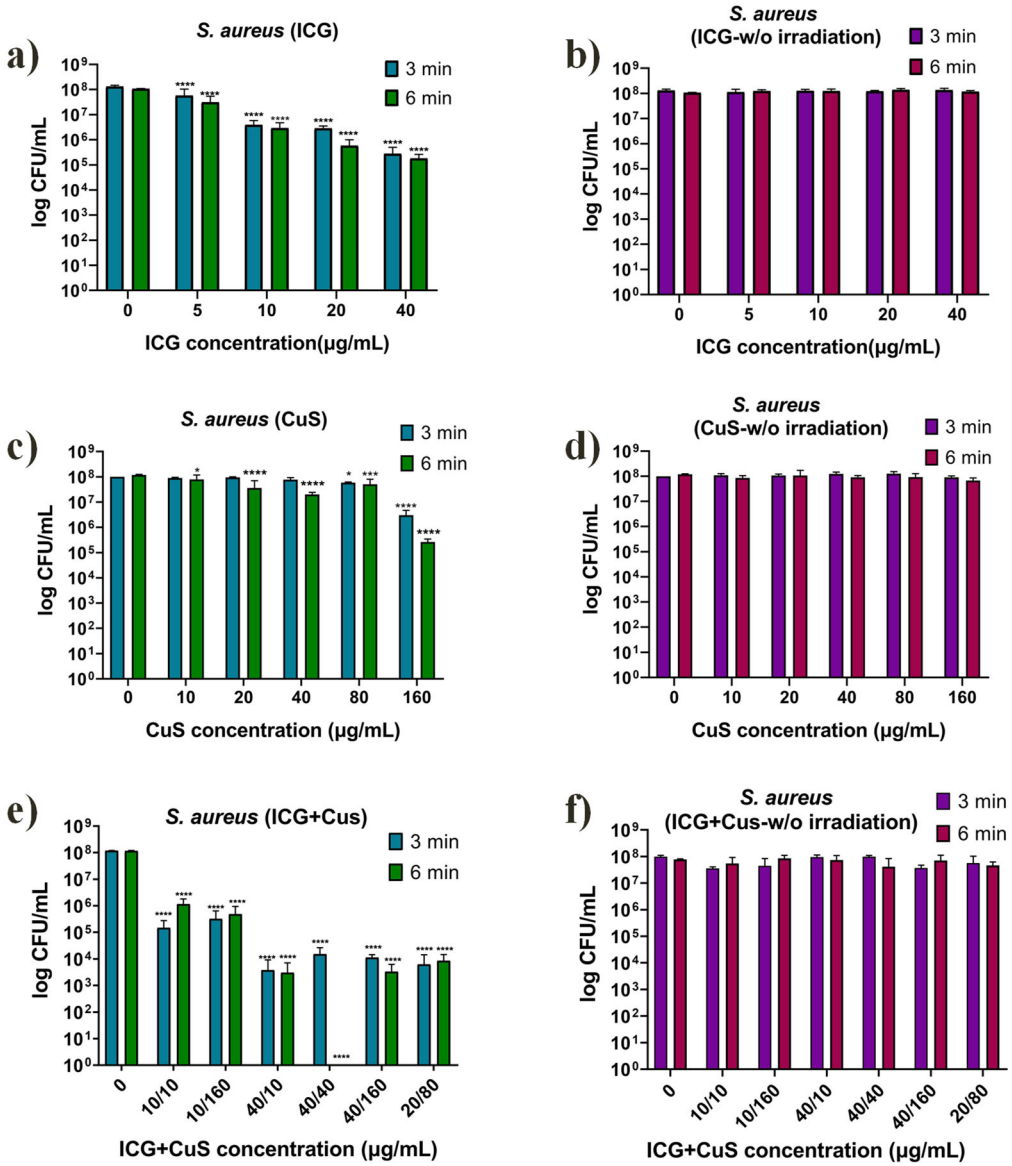

Fig. 2. (a) and (b) Antimicrobial effect of ICG for *S. aureus* irradiated (808 nm laser set at 1 W/cm^2 for 3 min and 6 min) (a) and incubated in darkness for the same times (b). (c) and (d) Antimicrobial effect of CuS nanoparticles for *S. aureus* irradiated (808 nm laser set at 1 W/cm^2 for 3 min and 6 min) (c) and incubated in darkness for the same times (d). (e) and (f) Antimicrobial effect of ICG+CuS for *S. aureus* irradiated (808 nm laser set at 1 W/cm^2 for 3 min and 6 min (e) and incubated in darkness for the same times (f). Data are presented as mean ± SD (n= 3). (*p< 0.05, **p<0.01, ***p< 0.001, and****p< 0.0001).

Fig. 2 shows the dose-dependent photodynamic effect on wild type *S. aureus* (Gram-positive in the presence or absence of NIR light at two different irradiation times. No toxic effect was observed in the absence of NIR light, but a dose-dependent response was observed after illumination (Fig. 2-a and c). Interestingly, the combination of ICG and CuS promotes a more acute toxicity against *S. aureus* than the individual counterparts, achieving a complete bacteria elimination after 6 min of irradiation for the 40/40 wt. ratio combination (Fig. 2-e). The bactericidal effect of ICG, CuS nanoparticles and their combination was also tested on *P. aeruginosa* (Gram-negative) with and without NIR laser irradiation (Fig. 3). The antimicrobial activity of both ICG and CuS increased with an increase in concentration and fluence. A reduction of 3-log in the CFU was achieved under 6 min of NIR irradiation of ICG and CuS at concentrations of 40 and 160 μg/mL respectively. Compared to *P. aeruginosa*, ICG showed a superior bactericidal effect on the *S. aureus* that can be attributed to the different structure of their cell-wall composition. For instance, at an ICG concentration of 20 μg/mL a 2-log reduction was observed after 6 min of irradiation on *S. aureus* whereas no differences were observed for *P. aeruginosa* compared to its control (Figs. 2a and 3a). The pKa of ICG is 3.27[49] and consequently under culture conditions ICG would carry a positively charged quaternary ammonium group and a negative net charge because both sulphonate groups in its structure would be deprotonated. In agreement with the previous literature, higher concentrations of ICG are needed to produce bactericidal effect on *P. aeruginosa* compared to the ones required to elicit antimicrobial effect on *S. aureus*, and it has been attributed to the reduced penetration of the negatively charged ICG in the Gram-negative bacteria studied due to the highly anionic nature of its outer membrane.[50] CuS nanoparticles exerted a similar antimicrobial effect on both bacteria (Figs. 2-3) and only at the highest concentration tested (160 μg/mL) they exhibited a 3-log reduction. At 80 μg/mL only 1-log reduction

was observed on *P. aeruginosa*, but this reduction was not considered as significant in the serial dilution method used. The antimicrobial photodynamic effect of those CuS nanoparticles was independent on the bacteria type probably caused by the lack of nanoparticle internalization inside of the bacteria (nanoparticle size ~ 200 nm) and the consequent generation of ROS in the extracellular space in close proximity to the bacteria. Jayawardena *et al.*[51] showed that non-functionalized silica nanoparticles (~80 nm), magnetic nanoparticles (~6 nm), silica-coated magnetic nanoparticles (~25 nm) and silica-coated quantum dots (~25 nm) were not internalized within four different strains of *E. coli*. As an example, the SecA subunit of the protein secretion complex in *E. coli* is the largest reported porin in its outer membrane with a size estimated in around 6 nm;[52] therefore, it is reasonable to think that particles of large sizes (*e.g.*, 200 nm in diameter for the CuS nanoparticles used in this work) would be excluded unless the nanoparticles cause disruption in the membrane and diffuse in the interior of partially damaged bacteria. Dai *et al.*[53] reported the antimicrobial activity of CuS nanoclustes coated with a thiazole derivative as a membrane-targeting cationic ligand. These CuS nanoclusters of 30 nm size anchored to the bacteria and produced an irreversibly damage to the bacterial membrane by the generation of ROS and heat upon irradiation, efficiently killing them. As we mentioned before, the lack of cellular uptake is an advantage because the chances of developing resistance are minimized. The longer the irradiation time and fluence, the higher the antimicrobial effect observed. As previously commented, the temperature of the cultures was monitored and this did not induce any photothermal damage, being the antimicrobial effect solely attributed to the photodynamic effect.

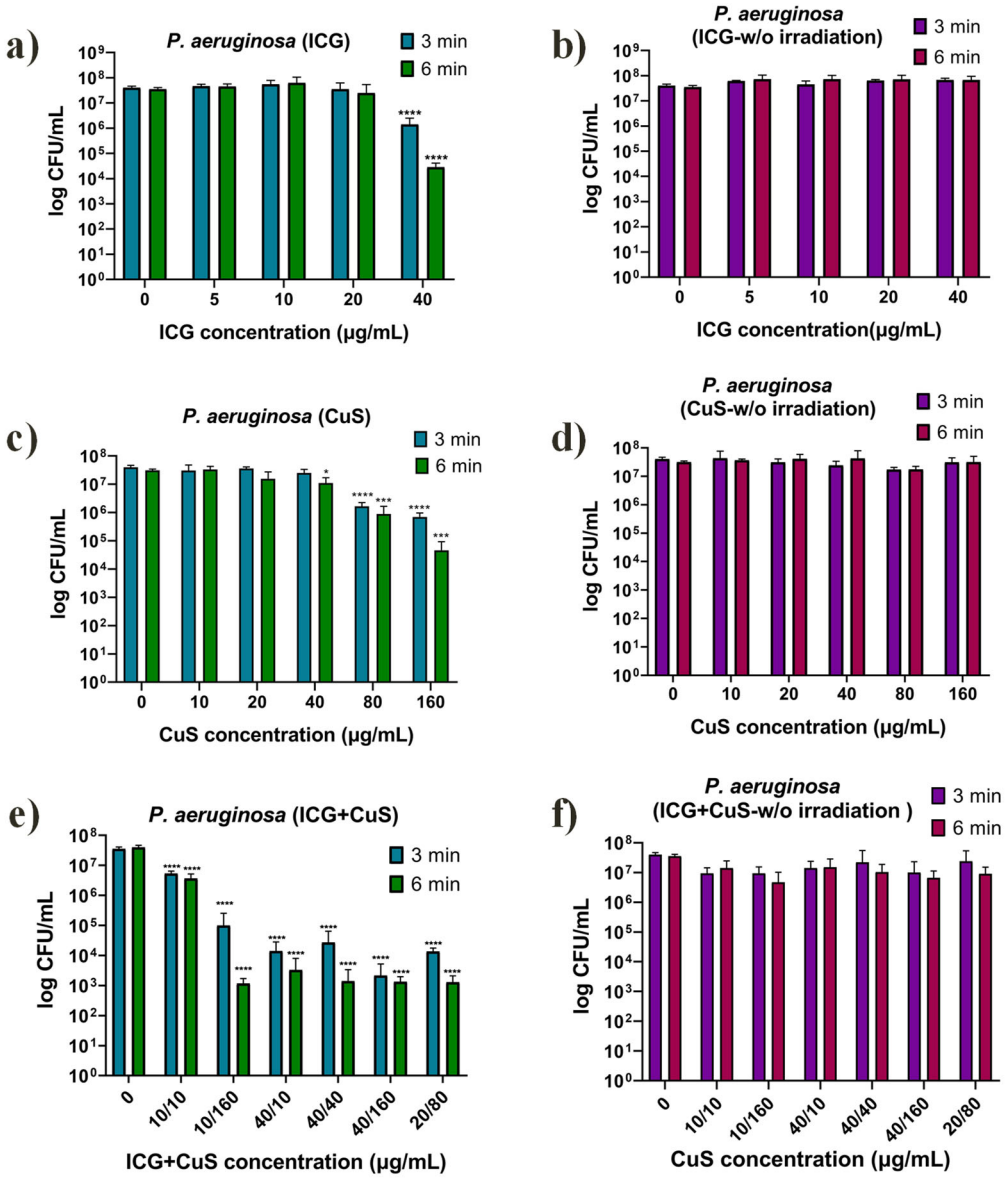

Fig. 3. (a) and (b) Antimicrobial effect of ICG for *P. aeruginosa* irradiated with an 808 nm laser set at 1 W/cm^2 for 3 min and 6 min (a) and incubated in darkness for the same times (b). (c) and (d) Bactericidal effect of CuS nanoparticles for *P. aeruginosa* irradiated with an 808 nm laser set at 1 W/cm^2 for 3 min and 6 min (c) and incubated in darkness for the same times (d). (e) and (f) Antimicrobial effect of ICG+CuS for *P. aeruginosa* irradiated with an 808 nm laser set at 1 W/cm^2 for 3 min and 6 min (e) and incubated in darkness for the same times (f). Data are presented as mean ± SD (n= 3). (*p< 0.05, **p<0.01, ***p< 0.001, and****p< 0.0001).

Fig. 2e-f shows the synergetic antimicrobial effect against *S. aureus* when combining both ICG and CuS nanoparticles. Different rations of both photosensitizers were analyzed, and we observed that a maximum in the antimicrobial effect against *S. aureus* was reached for the 40/40 μg/mL ratio. The increase in the concentration of CuS nanoparticles did not improve the antimicrobial effect any further probably because light scattering played an important role, and the light was unable to activate ICG and/or CuS. Absorption and scattering in aggregates are different than those in individual nanoparticles caused by the strong optical and electromagnetic interaction in the former. Light penetration depends on the interparticle distance in such a way that the closer the nanoparticles are placed, the shorter the light penetration depth is.[54] The light irradiated on the samples would be absorbed by the photosensitizer or absorbed and scattered by the CuS nanoparticles. In suspension, when the nanoparticle concentration increases the light does not penetrate as deeply into the dispersion and an increased backscattering off the fluid surface at high particle concentrations is observed.[55] Therefore, there was a tradeoff between the amount of CuS nanoparticles to be added to foster the antimicrobial effect of ICG and their ability to scatter the irradiating light. At high nanoparticle concentrations, part of that scattered light could be lost and unable to activate the generation of oxidative stress by both ICG and CuS. The same could be applied to ICG, increased amounts of the photosensitizer would produce a superior photodynamic effect until reaching concentration-quenching. Elevated concentrations of the ICG would produce a large number of molecular collisions and highly energetic vibrational modes of the fluorophore bonds, creating a channel for dissipation of excited state energy.[56] It is reasonable to think that in a real medical setting in the management of infected topical wounds backscattering would not play an important role because both photosensitizers would spread all around the surface of the skin being available to light activation.

A similar effect was observed on *P. aeruginosa* where high antimicrobial effect was reached for many of the different concentrations tested (Fig. 3e-f). Probably the intrinsic scattering of the bacteria themselves play a role being at the same concentration the culture of the *P. aeruginosa* more translucid than the one of *S. aureus* because of the characteristic golden-yellow color of the later.

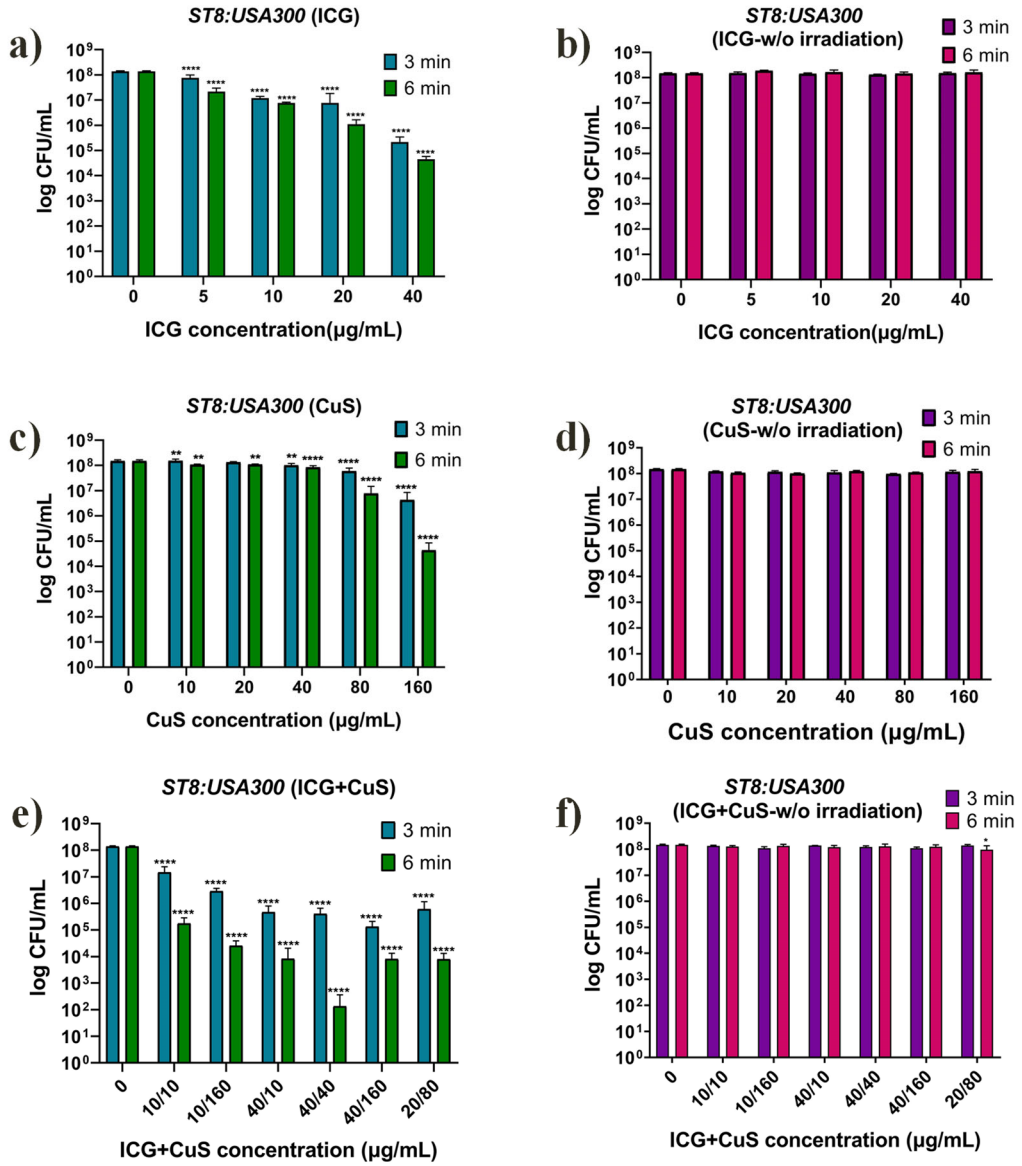

Fig. 4. (a) and (b) Antimicrobial effect of ICG for *S. aureus* USA300 irradiated (808 nm laser set at 1 W/cm^2 for 3 min and 6 min) (a) and incubated in darkness for the same times (b). (c) and (d) Antimicrobial effect of CuS NPs for *S. aureus* USA300 irradiated (808 nm laser set at 1 W/cm^2 for 3 min and 6 min) (c) and incubated in darkness for the same

times (d). (e) and (f) Antimicrobial effect of ICG+CuS for *S. aureus* USA300 irradiated (808 nm laser set at 1 W/cm^2 for 3 min and 6 min) (e) and incubated in darkness for the same times (f). Data are presented as mean ± SD (n= 3). (*p< 0.05, **p<0.01, ***p< 0.001, and****p< 0.0001).

Fig. 4 depicts the antimicrobial activity of the different materials against clinical isolates of methicillin-resistant *S. aureus*-USA300. We observed that the combined concentrations of CuS nanoparticles and ICG to reduce ST8-USA300 counts (Fig. 4e) were lower than the ones needed to exert the same action against the wild type *S. aureus* (Fig. 2e). No obvious correlation between photoinactivation and drug resistance has been previously reported[50] in agreement with our results. It can be seen in Fig. 4e that compared to the antimicrobial effect of ICG and CuS separately (Figs. 4a and c, respectively) a synergetic effect is observed when both materials were combined. Acute or chronic topical wounds infected with MRSA represent a serious clinical concern but the combination here reported together with the use of NIR light as activator of the oxidative stress would represent an effective non-invasive potential treatment. Again, a maximum bactericidal effect was obtained for the 40/40 ratio while a 3-log reduction was obtained even at the lowest dose tested (i.e., 10/10 ratio) after 6 min of irradiation. The influence of combined CuS nanoparticles and ICG (40+160 μg/mL) and irradiation (808 nm, 1 W/cm^2, 6 min) on *S. aureus* and *P. aeruginosa* was analyzed also by SEM (Fig. 5). SEM images of control samples (non-treated and non-irradiated) of *S. aureus* (Fig. 5a) and *P. aeruginosa* (Fig. 5c) showed their characteristic structure without clear damage on the cell wall. However, after treatment and irradiation, *S. aureus* and *P. aeruginosa*, (Fig. 5 b and d, respectively) showed disruption of the bacterial envelope and residues of debris and damaged bacteria were observed, consequence of the bactericidal effect of combined

ICG and CuS although the original morphology of some bacteria was also preserved. Energy-dispersive X-ray (EDX) spectra in *S. aureus*-treated samples corroborated the presence of Cu and S atoms coming from nanoparticles (Fig. S2).

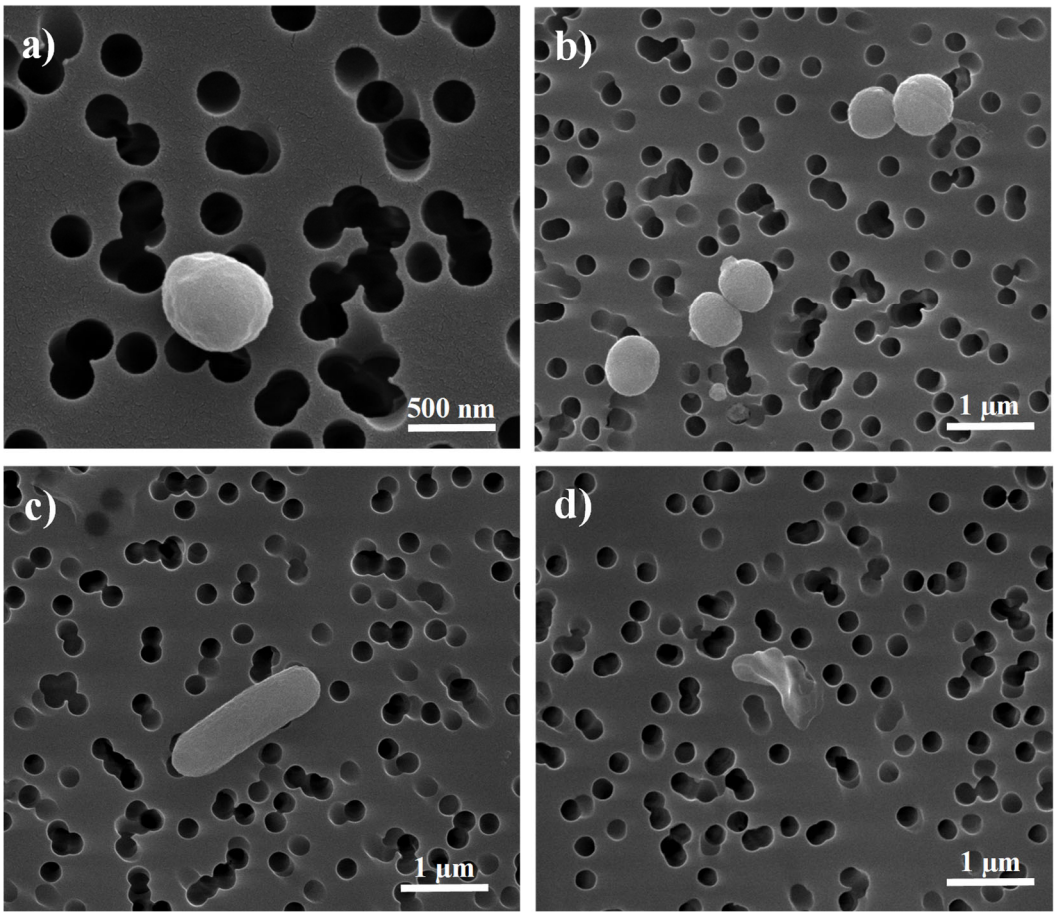

Fig. 5. SEM images of bacteria not treated and not irradiated (a) and (c), and treated with ICG+CuS 40+160 µg/mL (b) and (d). (a) Not treated and not irradiated and (b) irradiated (808 nm, 1 W/cm^2, 6 min) *S. aureus*. (c) Not treated and not irradiated and (d) irradiated (808 nm, 1 W/cm^2, 6 min) *P. aeruginosa*.

Once more, a synergetic effect was observed for *C. albicans* (Fig. 6). The combination of both ICG and CuS and light irradiation showed an antimicrobial dose-dependent trend which depends on the turbidity of the medium and its associated light scattering (Fig. 6e). High nanoparticle concentrations did not induce a superior antifungal effect but probably caused by the loss of photons due to scattering in the Eppendorf tubes used. The doses

required to exert antifungal action for both ICG and CuS nanoparticles independently were higher than those required to eliminate bacteria in agreement with the previous literature.[57] This fact is attributed to the presence of a nuclear envelope in fungi, which represents an additional barrier for the photosensitizer to diffuse in the cell interior, and to the larger size of fungi compared to bacteria (approx. 10 times larger) being the amount of ROS necessary to eliminate yeasts superior to the one needed to eliminate bacteria.[58] Demidova *et al.*[58] showed that the doses of photosensitizers (rose Bengal, toluidine blue O, and a poly-l-lysine chlorin(e6) conjugate) required were from 10 to 50 times higher to eliminate *C. albicans* (ATCC 18804) than the ones required to eliminate *E. coli* (ATCC 25922) and *S. aureus* (SA113). Superior anti-*C. albicans* biofilm effect was observed in the combination of gold nanoparticles and methylene blue, together with the disruption of yeast morphology as in our studies, attributed to the nonradiative energy decay by gold nanoparticles of the organic photosensitizer causing the transition to ground state, which resulted in the formation of hydroxyl free radicals.[59] Viana *et al*.[60] observed a reduction in the inactivation of *C. albicans* when an organic photosensitizer (meso-tetrakis (N-ethyl-2-pyridinium-2-yl) porphyrin) was conjugated on the surface of quantum dots and this was attributed to a reduced transmembrane cellular uptake of the conjugate compared to the free photosensitizer due to its size, reducing their photoactivity. In our case, there was no conjugation between both organic photosensitizer and CuS nanoparticles, and therefore both extracellular and intracellular spaces were targeted.

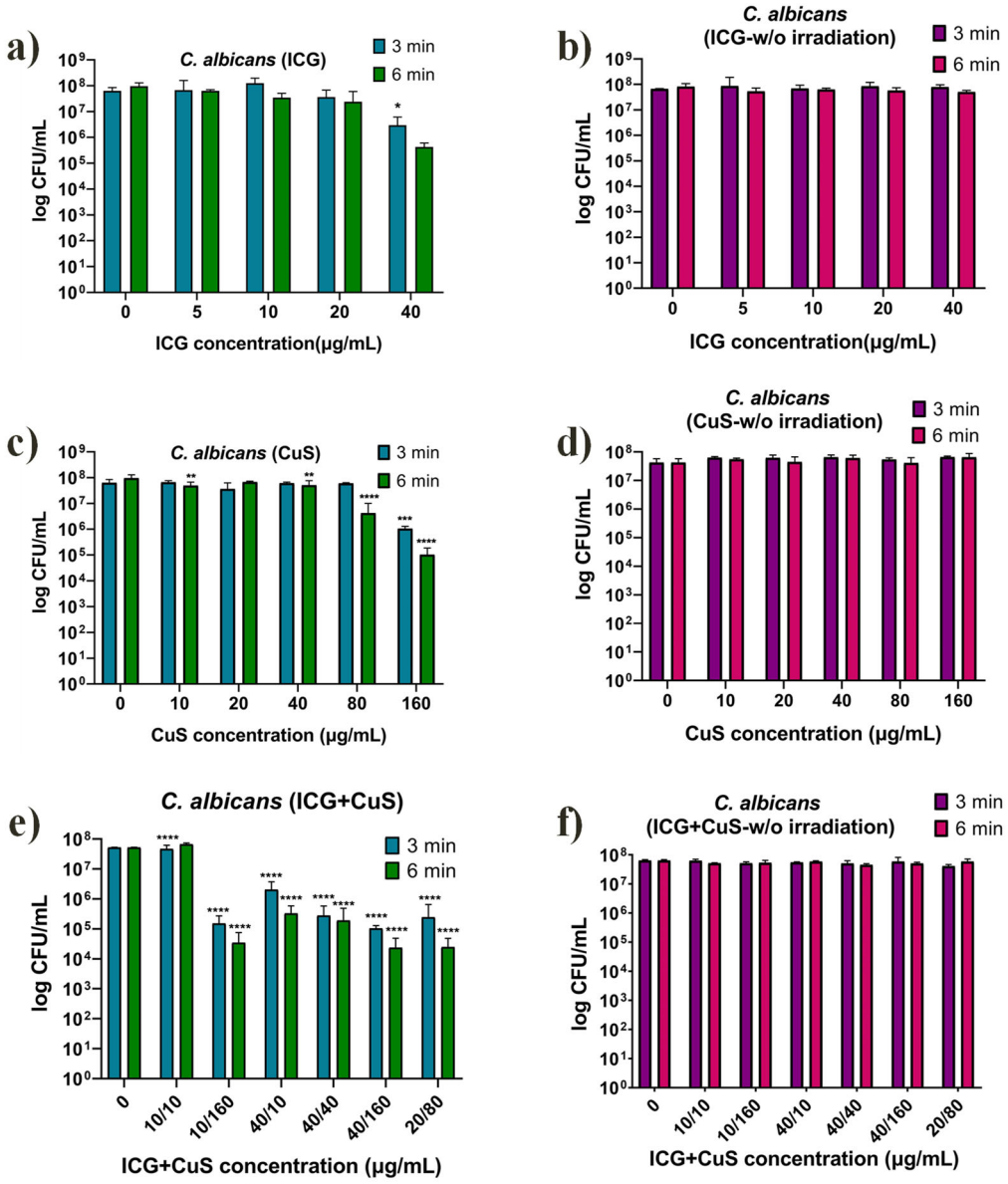

Fig. 6. (a) and (b) Antimicrobial effect of ICG for *C. albicans* irradiated (808 nm laser, 1 W/cm^2, 3 min and 6 min) (a) and incubated in darkness for the same times (b). (c) and (d) Antimicrobial effect of CuS NPs for *C. albicans* irradiated (808 nm laser, 1 W/cm^2, 3 min and 6 min) (c) and incubated in darkness for the same times (d). (e) and (f) Antimicrobial effect of ICG+CuS NPs for *C. albicans* irradiated (808 nm laser, 1 W/cm^2, 3 min and 6 min) (e) and incubated in the dark for the same times (f). Data are presented as mean ± SD (n= 3). (*p< 0.05, **p<0.01, ***p< 0.001, and****p< 0.0001).

To corroborate the photodynamic effect of ICG and CuS nanoparticles under NIR irradiation, enhanced ROS generation was confirmed through fluorescence intensity detection using the tracking agent DHR123. Fig. S3 shows the ROS production for ICG (40 μg/mL), CuS (40 μg/mL) and CuS+ICG (40+40 μg/mL) upon irradiation in the same conditions used for microbial suspensions (808 nm, 1 W/cm^2 during 6 min). The ROS yield notably increased upon NIR irradiation compared to the solutions heated at the equivalent temperature recorded during irradiation. The results confirmed that the enhancement in ROS production was attributed to the photodynamic effect induced by NIR laser absorption on ICG, CuS and CuS+ICG combination. Furthermore, the ROS yield in the combination of ICG and CuS was higher than the ROS production observed for individual ICG and CuS showing an additive trend. The synergetic photodynamic antimicrobial and antifungal effects observed in bacteria and fungi depended on the turbidity of the medium and its associated potential light scattering effect which would be detrimental for the ROS production. Light would scatter in media having high CuS nanoparticle concentration and those incident photons, without losing energy, would not irradiate the photosensitizer. Therefore, a tradeoff between the nanoparticle concentration in the dispersion and the photodynamic effect would be necessary to produce a synergetic photodynamic effect. Furthermore, the generation of singlet oxygen was measured using the fluorescence probe SOSG. Fig. S4 shows the results for the singlet oxygen determination using SOSG for ICG (40 μg/mL) and CuS (40 μg/mL). After irradiation under the same conditions used for the antimicrobial studies (808 nm, 1 W/cm^2, 6 min), both ICG and CuS nanoparticles yielded singlet oxygen as observed by the increase in the fluorescence of the SOSG probe. The generation of singlet oxygen supports the observed photodynamic antimicrobial effect, where ICG (40 μg/mL) produced a higher

amount of singlet oxygen than CuS nanoparticles (40 µg/mL), which may explain the superior antimicrobial effect of ICG for the microbes studied at the same concentration.

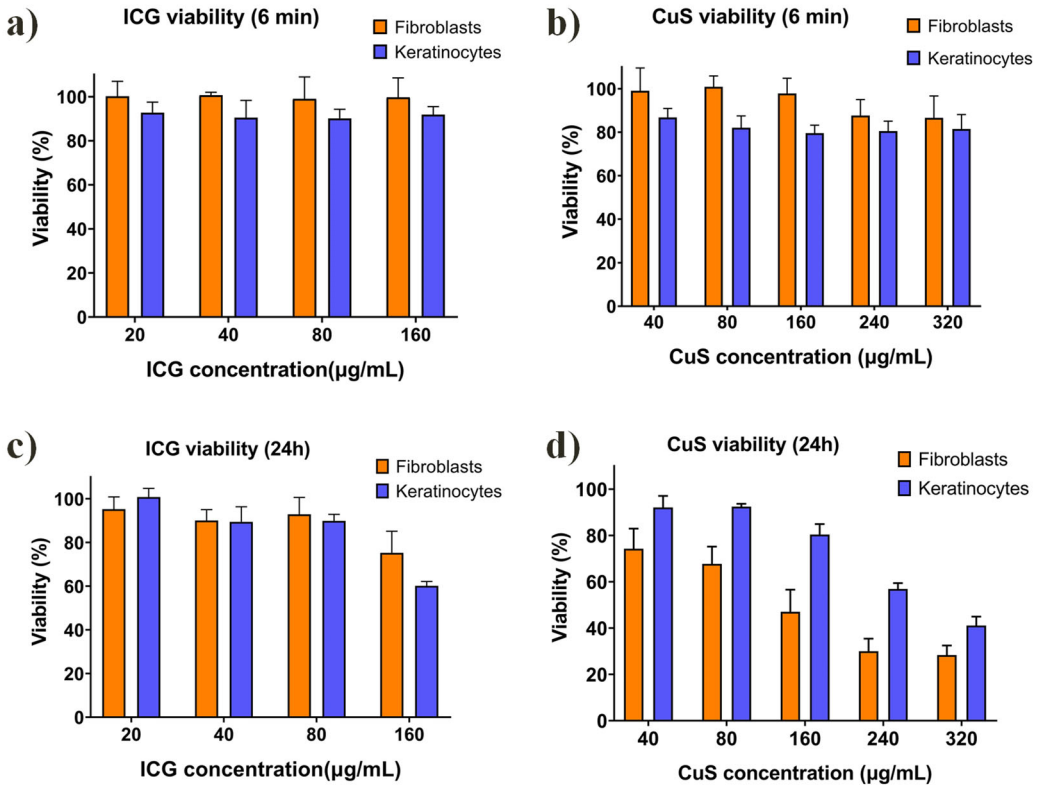

Fig. 7. Cytotoxicity of ICG (a, c) and CuS nanoparticles (b, d) when fibroblasts and keratinocytes were treated for 6 min (a, b) and 24h (c, d). Data represent mean ± SD of five experiments. Control samples (untreated cells) exerted 100% viability.

The cytotoxic effects of ICG (20-160 µg/mL) and CuS nanoparticle (40-320 µg/mL) treatment were also studied at two different time points (6 min and 24 h) in human dermal fibroblasts and keratinocytes. Fig. 7 shows the results obtained from the Blue Cell Viability assay. After cell treatment for 6 min (Figs. 7a and b), cell viability was slightly decreased though exerting viability percentages higher than 80%. When cells were treated with ICG for 24h (Fig. 7 c), cell viability was also higher than 80% except for the highest concentration assayed (160 µg/mL) at which fibroblasts displayed a viability percentage higher than 70% but keratinocytes decreased their viability showing percentages around 60%. These results are in line with previous studies in human Tenon´s fibroblasts which

also showed high viability and not impaired cell proliferation when cells were incubated with ICG at concentrations of 0.5% and below,[61] or when MH7A cells were treated with ICG concentrations up to 100 μg/mL.[62] Conversely, cell treatment with CuS nanoparticles for 24 h (Fig. 7d) involved higher cell toxicity showing percentages lower than 70% for fibroblasts and keratinocytes at concentrations from 160 μg/mL and 240 μg/mL, respectively. These results are in accordance with our previous results regarding fibroblasts toxicity after treatment with CuS nanoparticles for 24 h.[39] Considering these percentages, the results obtained in the dose-dependent photodynamic effect assays (Figs. 2-5) and the recommendations of the ISO 10993-5,[63] which indicates that percentages higher than 70% can be considered as subcytotoxic, 40 μg/mL of ICG and 160 μg/mL of CuS nanoparticles for 24 h were considered the subcytotoxic concentrations in the flow cytometry studies as these conditions were the bactericidal ones and in order to check their cytocompatibility on eukaryotic cells.

Flow cytometry assays (Tables 1 and 2; Figs. S5 and S6) confirmed these results showing apoptosis percentages (Table 1, Fig. S5) close to those exerted by the control sample (non-treated cells). In both cell types, apoptosis (early apoptosis + late apoptosis) was slightly increased (<13%) when cells were treated with CuS nanoparticles. In this regard, cell cycle (Table 2, Fig. S6) was more affected when CuS nanoparticles were added to the cultures than when ICG was present in the samples, slightly changing the distribution of cell cycle phases, as we previously described.[39]

Table 1. Apoptosis percentages obtained by flow cytometry

	Control	CuS Nanoparticles	ICG
	Fibroblasts (%)		
Viability	95.32	82.94	94.19
Early apoptosis	1.74	7.07	2.27
Late apoptosis	2.53	9.44	3.31

Necrosis	0.45	0.56	0.23
	Keratinocytes (%)		
Viability	90.42	85.61	90.93
Early apoptosis	2.52	7.39	3.62
Late apoptosis	5.26	6.73	5.23
Necrosis	1.80	0.27	0.22

Table 2. Cell cycle phases distribution obtained by flow cytometry

	Control	CuS Nanoparticles	ICG
	Fibroblasts (%)		
G1	28.84	77.73	34.80
S	34.84	17.04	28.86
G2	36.32	5.24	36.34
	Keratinocytes (%)		
G1	56.15	39.88	50.12
S	34.42	49.55	39.72
G2	9.42	10.58	10.16

4. Conclusions

A synergetic photodynamic antimicrobial effect was observed for the combination of an organic photosensitizer ICG and CuS nanoparticles. This effect was solely attributed to the generation of oxidative stress. The photodynamic effect of ICG, CuS and their combination was also demonstrated measuring the production of ROS. ICG can easily diffuse in the cellular cytosol and cause damage upon light stimulation, whereas CuS nanoparticles are largely excluded from the interior of the cells and its photodynamic effect would be exerted in the extracellular space. A dose-dependent effect was observed until reaching a maximum probably due to the optical shielding effect caused by the nanoparticles scattering. At high nanoparticle doses part of the irradiating light was backscattered without reaching the deepest part of the microbial suspensions. Herein we

have demonstrated the benefit of using the combination of organic photosensitizers and biodegradable semiconductor nanoparticles to eliminate bacteria and yeast based on intra- and extracellular oxidative stress. Cytocompability of the proposed photodynamic therapy was confirmed by cell culturing and flow cytometry studies which did not display significant detrimental effects for the cell lines involved in the intended clinical use of this therapy (fibroblasts and keratinocytes).

Conflicts of interest

The authors declare that they have no known competing financial interests or personal relationships that could have appeared to influence the work reported in this paper.

Acknowledgments

Financial support from Ministerio de Ciencia, Innovación y Universidades, Programa Retos Investigación, Proyecto REF: RTI2018-099019-A-I00 is gratefully acknowledged. This research was also funded by the Spanish Ministry of Economy and Competitiveness (grant number CTQ2017-84473-R). CIBER-BBN is an initiative funded by the VI National R&D&I Plan 2008–2011, Iniciativa Ingenio 2010, Consolider Program, CIBER Actions and financed by the Instituto de Salud Carlos III (Spain) with assistance from the European Regional Development Fund. We acknowledge the LMA-INA (University of Zaragoza, Spain). G.M. acknowledges the support from the Miguel Servet Program (MS19/00092; Instituto de Salud Carlos III).

References

1. S. Kwiatkowski, B. Knap, D. Przystupski, J. Saczko, E. Kedzierska, K. Knap-Czop, J. Kotlinska, O. Michel, K. Kotowski and J. Kulbacka, *Biomed. Pharmacother.*, 2018, **106**, 1098-1107.
2. Photodynamic Therapy for Cancer - National Cancer Institute. https://www.cancer.gov/about-cancer/treatment/types/surgery/photodynamic-fact-sheet (accessed Oct. 16).
3. M. R. Hamblin and T. Hasan, *Photochem. Photobiol. Sci.*, 2004, **3**, 436-450.
4. Y. Nitzan, M. Gutterman, Z. Malik and B. Ehrenberg, *Photochem. Photobiol.*, 1992, **55**, 89-96.

5. S. George, M. R. Hamblin and A. Kishen, *Photochem. Photobiol. Sci.*, 2009, **8**, 788-795.
6. R. F. Donnelly, P. A. McCarron and M. M. Tunney, *Microbiol. Res.*, 2008, **163**, 1-12.
7. F. Cieplik, D. Deng, W. Crielaard, W. Buchalla, E. Hellwig, A. Al-Ahmad and T. Maisch, *Crit. Rev. Microbiol.*, 2018, **44**, 571-589.
8. V. Perez-Laguna, I. Garcia-Luque, S. Ballesta, L. Perez-Artiaga, V. Lampaya-Perez, A. Rezusta and Y. Gilaberte, *Photodiagnosis Photodyn. Ther.*, 2020, **31**, 5.
9. J. Almeida, J. P. C. Tome, M. Neves, A. C. Tome, J. A. S. Cavaleiro, A. Cunha, L. Costa, M. A. F. Faustino and A. Almeida, *Photochem. Photobiol. Sci.*, 2014, **13**, 626-633.
10. V. Perez-Laguna, Y. Gilaberte, M. I. Millan-Lou, M. Agut, S. Nonell, A. Rezusta and M. R. Hamblin, *Photochem. Photobiol. Sci.*, 2019, **18**, 1020-1029.
11. M. R. Hamblin, *Expert Rev. Anti-Infect. Ther.*, 2017, **15**, 1059-1069.
12. L. Y. Huang, T. G. St Denis, Y. Xuan, Y. Y. Huang, M. Tanaka, A. Zadlo, T. Sarna and M. R. Hamblin, *Free Radic. Biol. Med.*, 2012, **53**, 2062-2071.
13. L. H. Chen, H. T. Bai, J. F. Xu, S. Wang and X. Zhang, *ACS Appl. Mater. Interfaces*, 2017, **9**, 13950-13957.
14. F. Berthiaume, S. R. Reiken, M. Toner, R. G. Tompkins and M. L. Yarmush, *Bio-Technology*, 1994, **12**, 703-706.
15. X. M. Lu, A. J. Fischman, E. Stevens, T. T. Lee, L. Strong, R. G. Tompkins and M. L. Yarmush, *J. Immunol. Methods*, 1992, **156**, 85-99.
16. M. L. Embleton, S. P. Nair, W. Heywood, D. C. Menon, B. D. Cookson and M. Wilson, *Antimicrob. Agents Chemother.*, 2005, **49**, 3690-3696.
17. R. Dosselli, C. Tampieri, R. Ruiz-Gonzalez, S. De Munari, X. Ragas, D. Sanchez-Garcia, M. Agut, S. Nonell, E. Reddi and M. Gobbo, *J. Med. Chem.*, 2013, **56**, 1052-1063.
18. F. Liu, A. S. Y. Ni, Y. Lim, H. Mohanram, S. Bhattacharjya and B. G. Xing, *Bioconjugate Chem.*, 2012, **23**, 1639-1647.
19. S. Parker, *Br. Dent. J.*, 2013, **215**, 167-171.
20. M. Wainwright, T. Maisch, S. Nonell, K. Plaetzer, A. Almeida, G. P. Tegos and M. R. Hamblin, *The Lancet. Infectious diseases*, 2017, **17**, e49-e55.
21. M. Ochsner, *J. Photochem. Photobiol. B-Biol.*, 1997, **39**, 1-18.
22. I. Georgakoudi, M. G. Nichols and T. H. Foster, *Photochem. Photobiol.*, 1997, **65**, 135-144.
23. S. Perni, P. Prokopovich, J. Pratten, I. P. Parkin and M. Wilson, *Photochem. Photobiol. Sci.*, 2011, **10**, 712-720.
24. R. Yin, T. Agrawal, U. Khan, G. K. Gupta, V. Rai, Y. Y. Huang and M. R. Hamblin, *Nanomedicine*, 2015, **10**, 2379-2404.
25. T. T. Yao, J. Wang, Y. F. Xue, W. J. Yu, Q. Gao, L. Ferreira, K. F. Ren and J. Ji, *J. Mat. Chem. B*, 2019, **7**, 5089-5095.
26. D. Mao, F. Hu, Kenry, S. L. Ji, W. B. Wu, D. Ding, D. L. Kong and B. Liu, *Adv. Mater.*, 2018, **30**, 7.
27. C. M. B. Carvalho, E. Alves, L. Costa, J. P. C. Tome, M. A. F. Faustino, M. Neves, A. C. Tome, J. A. S. Cavaleiro, A. Almeida, A. Cunha, Z. Lin and J. Rocha, *ACS Nano*, 2010, **4**, 7133-7140.
28. J. Schwiertz, A. Wiehe, S. Grafe, B. Gitter and M. Epple, *Biomaterials*, 2009, **30**, 3324-3331.
29. A. Shrestha, M. R. Hamblin and A. Kishen, *Nanomed.-Nanotechnol. Biol. Med.*, 2014, **10**, 491-501.

30. S. W. Li, S. S. Cui, D. Y. Yin, Q. Y. Zhu, Y. X. Ma, Z. Y. Qian and Y. Q. Gu, *Nanoscale*, 2017, **9**, 3912-3924.
31. M. Prieto, A. Y. Rwei, T. Alejo, T. Wei, M. T. Lopez-Franco, G. Mendoza, V. Sebastian, D. S. Kohane and M. Arruebo, *ACS Appl. Mater. Interfaces*, 2017, **9**, 41737-41747.
32. Y. X. Zhang, P. Huang, D. Wang, J. C. Chen, W. Z. Liu, P. Hu, M. D. Huang, X. Y. Chen and Z. Chen, *Nanoscale*, 2018, **10**, 15485-15495.
33. Z. L. Zhou, S. S. Peng, M. H. Sui, S. G. Chen, L. S. Huang, H. Xu and T. T. Jiang, *Colloid Surf. B-Biointerfaces*, 2018, **161**, 394-402.
34. Z. Yuan, B. L. Tao, Y. He, C. Y. Mu, G. H. Liu, J. X. Zhang, Q. Liao, P. Liu and K. Y. Cai, *Biomaterials*, 2019, **223**, 15.
35. J. Zhou, Z. Hu, F. Zabihi, Z. Chen and M. Zhu, *Adv. Fiber Mater.*, 2020, **2**, 123-139.
36. M. C. A. de Oliveira, F. A. G. da Silva, M. M. da Costa, N. Rakov and H. P. de Oliveira, *Adv. Fiber Mater.*, 2020, **2**, 256-264.
37. A. Contreras, M. J. Raxworthy, S. Wood, J. D. Schiffman and G. Tronci, *ACS Appl. Bio Mater.*, 2019, **2**, 4258-4270.
38. L. R. Guo, I. Panderi, D. D. Yan, K. Szulak, Y. J. Li, Y. T. Chen, H. Ma, D. B. Niesen, N. Seeram, A. Ahmed, B. F. Yan, D. Pantazatos and W. Lu, *ACS Nano*, 2013, **7**, 8780-8793.
39. I. O. de Solorzano, M. Prieto, G. Mendoza, T. Alejo, S. Irusta, V. Sebastian and M. Arruebo, *ACS Appl. Mater. Interfaces*, 2016, **8**, 21545-21554.
40. K. Bilici, N. Atac, A. Muti, I. Baylam, O. Dogan, A. Sennaroglu, F. Can and H. Y. Acar, *Biomater. Sci.*, 2020, **8**, 4616-4625.
41. S. Ramadan, L. R. Guo, Y. J. Li, B. F. Yan and W. Lu, *Small*, 2012, **8**, 3143-3150.
42. I. O. de Solorzano, T. Alejo, M. Abad, C. Bueno-Alejo, G. Mendoza, V. Andreu, S. Irusta, V. Sebastian and M. Arruebo, *J. Colloid Interface Sci.*, 2019, **533**, 171-181.
43. M100Ed30 | Performance Standards for Antimicrobial Susceptibility Testing, 30th Edition. https://clsi.org/standards/products/microbiology/documents/m100/ (accessed Oct. 16, 2020).
44. G. Mendoza, A. Regiel-Fut.yra, V. Andreu, V. Sebastian, A. Kyziol, G. Stochel and M. Arruebo, *ACS Appl. Mater. Interfaces*, 2017, **9**, 17693-17701.
45. R. Philip, A. Penzkofer, W. Baumler, R. M. Szeimies and C. Abels, *J. Photochem. Photobiol. A-Chem.*, 1996, **96**, 137-148.
46. Y. Shafiei, V. Razavilar and A. Javadi, *Aust. J. Basic & Appl. Sci*, 2011, **5**, 1551-1554.
47. B. E. Smith, P. B. Roder, X. Z. Zhou and P. J. Pauzauskie, *Nanoscale*, 2015, **7**, 7115-7126.
48. G. Shafirstein, W. Baumler, L. J. Hennings, E. R. Siegel, R. Friedman, M. A. Moreno, J. Webber, C. Jackson and R. J. Griffin, *Int. J. Cancer*, 2012, **130**, 1208-1215.
49. O. G. Bjornsson, R. Murphy and V. S. Chadwick, *Experientia*, 1982, **38**, 1441-1442.
50. N. Topaloglu, M. Gulsoy and S. Yuksel, *Photomed. Laser Surg.*, 2013, **31**, 155-162.
51. H. S. N. Jayawardena, K. W. Jayawardana, X. Chen and M. D. Yan, *Chem. Commun.*, 2013, **49**, 3034-3036.
52. H. W. Wang, Y. Chen, H. C. Yang, X. C. Chen, M. X. Duan, P. C. Tai and S. F. Sui, *Proc. Natl. Acad. Sci. U. S. A.*, 2003, **100**, 4221-4226.

53. X. M. Dai, Y. Zhao, Y. J. Yu, X. L. Chen, X. S. Wei, X. G. Zhang and C. X. Li, *ACS Appl. Mater. Interfaces*, 2017, **9**, 30470-30479.
54. A. Garcia-Valenzuela, R. Marquez-Islas and R. G. Barrera, *Appl. Phys. A-Mater. Sci. Process.*, 2017, **123**, 8.
55. N. J. Hogan, A. S. Urban, C. Ayala-Orozco, A. Pimpinelli, P. Nordlander and N. J. Halas, *Nano Lett.*, 2014, **14**, 4640-4645.
56. S. Boddington, E. J. Sutton, E. Jones, D. D. Purcell, T. D. Henning, S. Tavri, R. Meier, A. Sista, Y. Fu and H. Daldrup-Link, *Contrast Media Mol. Imaging*, 2008, **3**, 191-197.
57. T. N. Demidova and M. R. Hamblin, *Int. J. Immunopathol. Pharmacol.*, 2004, **17**, 245-254.
58. T. N. Demidova and M. R. Hamblin, *Antimicrob. Agents Chemother.*, 2005, **49**, 2329-2335.
59. S. Khan, F. Alam, A. Azam and A. U. Khan, *Int. J. Nanomed.*, 2012, **7**, 3245-3257.
60. O. S. Viana, M. S. Ribeiro, A. C. D. Rodas, J. S. Reboucas, A. Fontes and B. S. Santos, *Molecules*, 2015, **20**, 8893-8912.
61. G. Reeves, R. Wallis, J. G. Crowston, K. M. Small and A. P. Wells, *J. Glaucoma*, 2007, **16**, 479-482.
62. Q. Tang, J. Y. Cui, Z. H. Tian, J. C. Sun, Z. G. Wang, S. F. Chang and S. Y. Zhu, *Int. J. Nanomed.*, 2017, **12**, 381-393.
63. ISO 10993-5:2009 - Biological Evaluation of Medical Devices. Part 5: Tests for In Vitro Cytotoxicity. http://www.iso.org/iso/catalogue_detail.htm?csnumber=36406).